Prediction uncertainty in elevation and its effect on flood inundation modelling

M.D. Wilson[1], P.M Atkinson[2]

[1] School of Geographical Sciences, University of Bristol,
University Road, Bristol BS8 1SS, UK.
Email: M.D.Wilson@bristol.ac.uk
[2] School of Geography, University of Southampton,
Highfield, Southampton SO17 1BJ, UK.
Email: P.M.Atkinson@soton.ac.uk

Abstract

In this paper, combined contour and Differential Global Positioning System (DGPS) data were used to predict elevation on the floodplain, for use in flood inundation models. The effect of prediction uncertainty in elevation on the prediction of flood inundation was assessed by generating multiple Digital Elevation Models (DEMs) through conditional simulation. Each DEM honoured the original data, and maintained the same spatial structure. Flood inundation was then predicted for each DEM using the grid-based model LISFLOOD-FP. The effects of prediction uncertainty in elevation increased with distance downstream and became compounded through time.

1. Introduction

Flood awareness in the UK has risen dramatically in the last few years after several major flood events. Research on flooding has seen a resurgence and, in particular, research has become increasingly focused on flood inundation modelling. However, all data used (and hence parameters and variables) in flood inundation models have inherent uncertainty. The challenge is to quantify this uncertainty and, perhaps more importantly, assess the effect that uncertainty may have on model predictions.

Floodplain topography is the principal variable that affects the movement of the flood wave and is, therefore, critical to the prediction of inundation extent. A small degree of uncertainty in elevation may have a relatively large effect on model predictions. Ideally, a flood inundation model requires elevation data that represent closely the true ground surface. High quality remotely-sensed elevation data are often unavailable for the area of interest and may contain features higher than the true land surface (e.g., buildings and vegetation). Any land feature which restricts (but not prevents) the flow of water (e.g. forest) should be accounted for in the friction terms of the model rather than represented by an area of higher elevation.

In this paper, readily available contour data were supplemented with Differential Global Positioning System (DGPS) measurements of elevation on the floodplain. To assess the effect of elevation prediction uncertainty on inundation extent, multiple plausible digital elevation models (DEMs) were generated. Each DEM was then used to predict flood inundation for the Easter 1998 flood event on the river Nene, Northamptonshire, England, using the grid-based model LISFLOOD-FP.

2. LISFLOOD-FP model of flood inundation

LISFLOOD-FP is a raster-based flood inundation model (Bates and De Roo, 2000; De Roo et al., 2000; Horritt and Bates, 2001). Channel flow is approximated using the 1D linear kinematic Saint-Venant equations (e.g. Chow et al., 1988). Cells in the domain that are identified as channel are incised by the bankfull depth, and a hydrograph is routed downstream from the domain inflow. When channel depth reaches a cell bankfull level, flood inundation commences.

Flow on the floodplain is based on a simple continuity equation, which states that the change in volume in a cell over time is equal to the fluxes into and out of it (Bates and De Roo, 2000):

$$\frac{dV}{dt} = Q_{up} + Q_{down} + Q_{left} + Q_{right} \tag{1}$$

where V is the volume of water in a cell, and Q_{up}, Q_{down}, Q_{left} and Q_{right} represent flow rates in each direction into (positive Q) and out of (negative Q) the cell. Flow rates are calculated based on the height of the water surface above the land, and the Manning friction coefficient:

$$Q_{i,j} = \frac{A_{i,j} R_{i,j}^{2/3} S_{i,j}^{1/2}}{n} \tag{2}$$

where $Q_{i,j}$ is the flux between two cells i and j, $A_{i,j}$ is the cross-sectional area at the cell interface, $R_{i,j}$ is the hydraulic radius at the cell interface, $S_{i,j}$ is the free surface slope between the two cells, and n is the Manning friction coefficient (see Chow, 1959; Chow et al., 1988). The cross-sectional area, $A_{i,j}$, is defined by (Horritt and Bates, 2001):

$$A_{i,j} = \left(\left| h_{i,j} \right|_{\max} - \left| z_{i,j} \right|_{\max} \right) \Delta x \tag{3}$$

where $\left| z_{i,j} \right|_{\max}$ is the maximum bed surface elevation between cells i and j, and $\left| h_{i,j} \right|_{\max}$ is the maximum water surface elevation (bed surface elevation plus water depth). The cross sectional area is divided by the wetted perimeter to give the hydraulic radius, $R_{i,j}$:

$$R_{i,j} = \frac{\left(\left| h_{i,j} \right|_{\max} - \left| z_{i,j} \right|_{\max} \right) \Delta x}{\Delta x + 2\left(\left| h_{i,j} \right|_{\max} - \left| z_{i,j} \right|_{\max} \right)} \tag{4}$$

Finally, slope, $S_{i,j}$, is calculated on the free water surface using:

$$S_{i,j} = \frac{\left(h_i - h_j \right)}{\Delta x} \tag{5}$$

To prevent more water leaving a cell than it contains, flow rates out of drying cells are scaled using a non-dimensional coefficient, c (Bates and De Roo, 2000):

$$c = \frac{V_t}{\left(Q_{up} + Q_{down} + Q_{left} + Q_{right} \right) \Delta t} \tag{6}$$

where V_t is the volume of water in a cell at time t. Thus, as the cell dries out depth returns to zero. Only drying cells are scaled in this way, and to preserve mass-balance inflows are not scaled.

The advantage of a simple flood inundation scheme (such as that used in LISFLOOD-FP) over finite element models (such as TELEMAC 2D) is its computational efficiency, with approximately 40 times fewer floating-point operations per cell, per time step (Bates and De

Roo, 2000). Further, the use of a raster data structure makes the incorporation of multiple data sets in the model relatively straightforward, particularly from remotely sensed sources.

3. Elevation data

Land-form PROFILE^{TM} contour data were obtained from the Ordnance Survey, and were then supplemented by Differential Global Positioning System (DGPS) measurements. A Trimble ProXRS GPS unit was used to gather elevation measurements along the channel and across the floodplain. The ProXRS is a 12 channel unit with carrier-phase filtered measurements, able to obtain sub-metre accuracy in all directions. The location of DGPS measurements in relation to the contour data is shown in Figure 1. Measurements were obtained on foot along accessible paths along the channel and across the floodplain, and by car along roads in the area. Some problems were encountered in wooded areas as a clear line of sight is needed between the DGPS unit and the satellite platforms. However, as large parts of the area are open, it was still possible to cover a wide area.

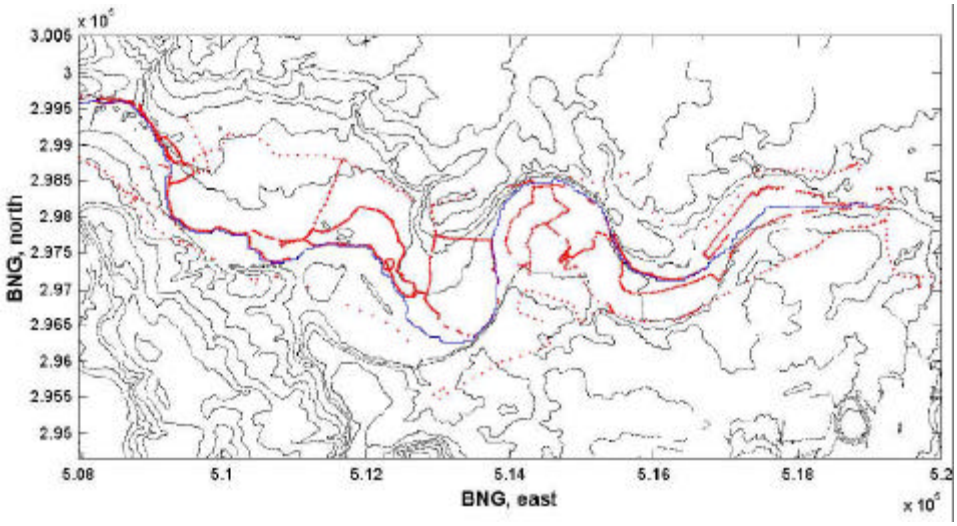

Figure 1. Location of contour data (black) and DGPS measurements (red) for the area used in Nene site simulations. Channel location is shown in blue.

Experimental variograms were predicted for the PROFILE^{TM} contour data, both inclusive and exclusive of the DGPS measurements (Figure 2a). In addition, areas above the 15 m contour line were removed and variograms predicted (Figure 2b). In both cases, the inclusion of DGPS with the PROFILE^{TM} contour data increased the variance. For the area below the 15 m contour line, the inclusion of DGPS data increased the variance at shorter lags than globally. The increase in spatial variation may indicate that the new data set is more representative of the floodplain, and, therefore, more suitable for use in flood inundation modelling.

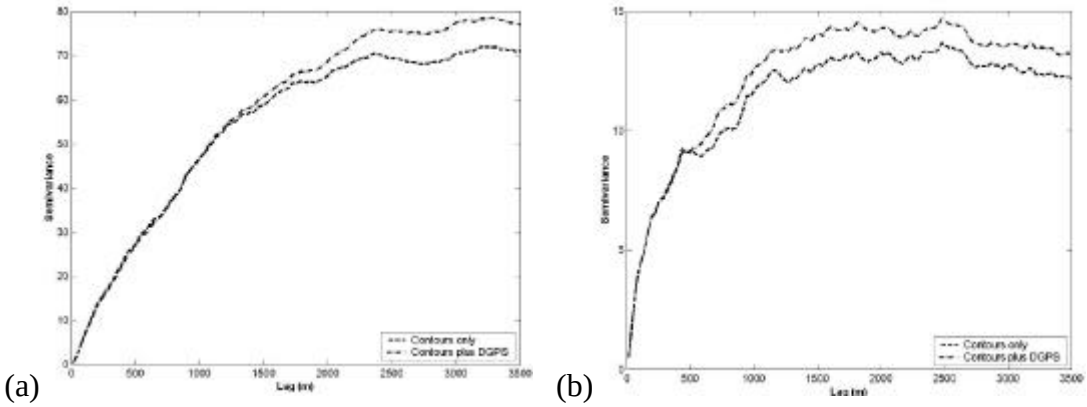

Figure 2. Variograms of PROFILE^{TM} contour data, and PROFILE^{TM} contour data after the inclusion of additional DGPS measurements, (a) for the full area, and (b) for the floodplain area below the 15 m contour line.

4. Generation of elevation scenarios

Spatial prediction uncertainty in the combined PROFILE^{TM} contour and DGPS data was assessed using the geostatistical method of stochastic imaging or conditional simulation. This enabled the sensitivity of LISFLOOD-FP to small changes in topography to be assessed. Conditional simulation (Deutsch & Journel 1998) was used to generate elevation scenarios as it honours the values of the data at their original locations (Figure 1), and aims to reproduce global features and statistics of the data. In particular, each simulation aims to maintain the same original variogram. Therefore, given the original data, each simulation can be said to have an equal probability of representing the true floodplain surface. Importantly, each simulation is superior to a Kriged surface, which is not a possible reality: by predicting optimally (i.e., taking the most probable value from the posterior distribution), Kriging produces a smoothed surface with a variogram very different to that of the original data (Goovaerts 1997). In addition, conditional simulation is superior to methods such as Monte Carlo simulation which do not maintain the spatial structure of the data.

One hundred different (but equally probable) elevation scenarios from the combined PROFILE^{TM} contour and DGPS data were generated using the Sequential Gaussian simulation (SGSim) program, part of the GSLIB software package (Deutsch & Journel 1998). The original variogram of the combined PROFILE^{TM} contour and DGPS data was used (Figure 2a). The standard deviation of all the DEMs generated is shown in Figure 3. Standard deviation is low in the vicinity of data points, and progressively rises with increased distance (and, hence, increased uncertainty). Figure 4 shows a smaller area of floodplain for clarity. By comparing model results obtained using the multiple elevation scenarios generated, the effect of spatial prediction uncertainty on the prediction of flood inundation was assessed.

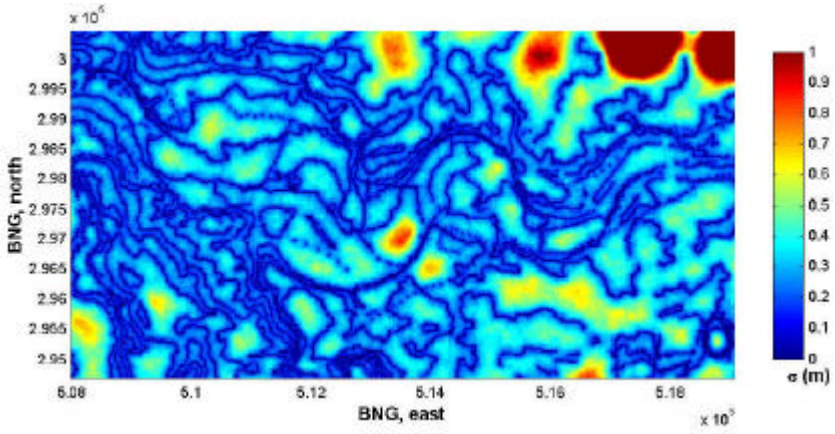

Figure 3. Standard deviation of elevation scenarios generated using sequential Gaussian simulation.

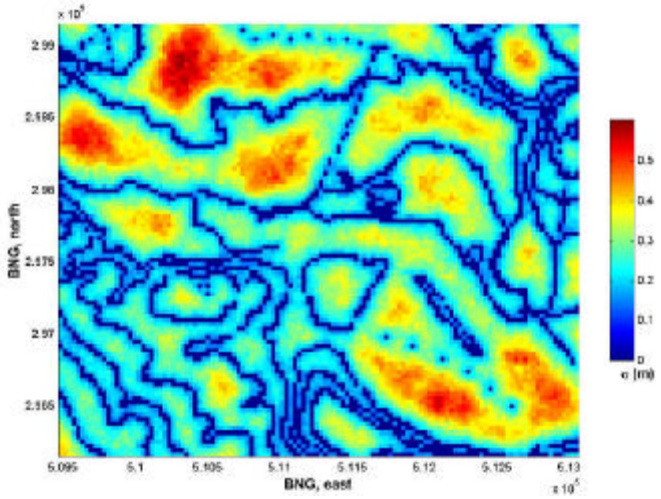

Figure 4. Standard deviation of elevation scenarios for a smaller area of floodplain, generated using sequential Gaussian simulation.

5. Sensitivity of LISFLOOD-FP to predicted elevation

All one hundred elevation scenarios were used to predict inundation, on a large Beowulf cluster at the University of Southampton. The standard deviation and coefficient of variation (CV) of inundation depth at the flood peak (80 hours) is shown in Figure 5. Only flooded cells were included in the calculations, which prevented non-flooded cells from skewing the results. Cells which were not flooded in some simulations would have decreased both the standard deviation and CV.

Variation in predicted inundation depth was generally greatest in areas of large elevation uncertainty. For example, the maximum standard deviation in depth was ~0.8 m at BNG 513,500 E, 297,000 N, which corresponded well with the higher standard deviation in elevation for the same area. In addition, along some lines of small elevation uncertainty, variation in predicted flood depth was correspondingly low. This was not always the case, however, as the pattern was highly complex. Points of small elevation uncertainty may still have resulted in a variable prediction of flood depth due to the surrounding topography. When mean depth was taken into account using the CV, it was the shallowest areas (particularly at the edge of the flood envelope) that exhibited the greatest variation in depth.

Uncertainty at the edge of the flood envelope was also observed by calculating the percentage of simulations in which each cell was flooded at the flood peak (Figure 6). A shallow gradient at the edge of the floodplain resulted in an uncertain prediction of flood extent, such as in the area at BNG 512,000 E, 298,500 N. Conversely, areas with steep slope at the edge of the floodplain (such as the outside of the meander bend at BNG 514,500 E, 298,750 N) have a high degree of certainty in flood extent.

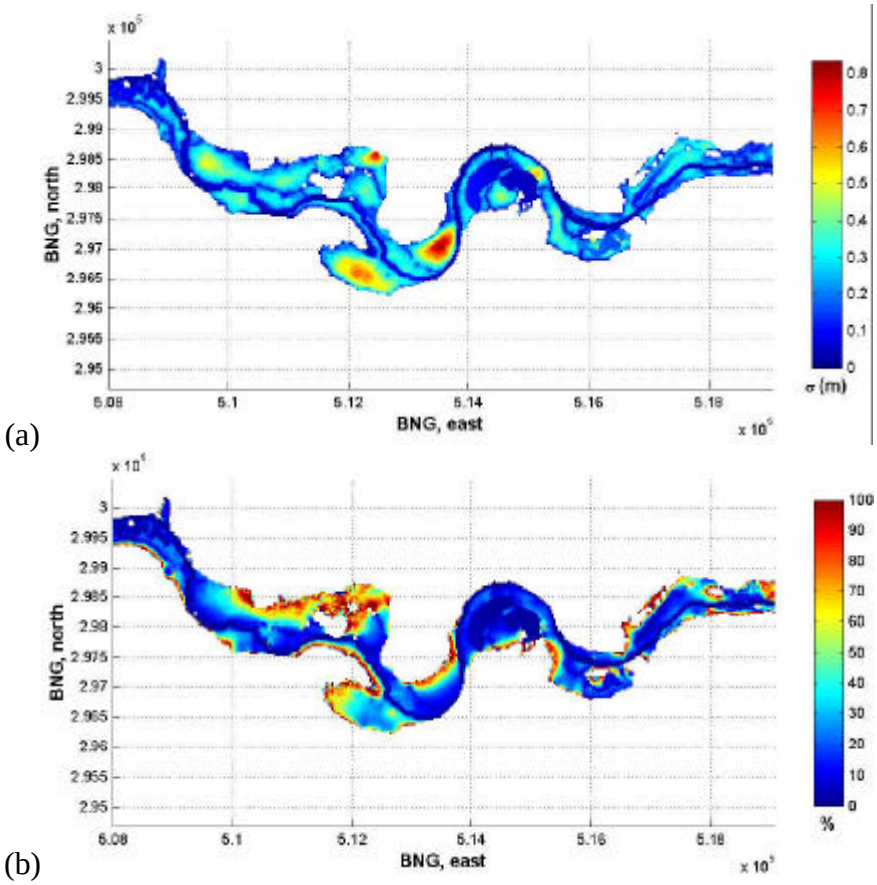

Figure 5. Variation in depth at flood peak (80 hours): (a) standard deviation, and (b) coefficient of variation. Non-flooded cells in each simulation were discounted to avoid skewing the results.

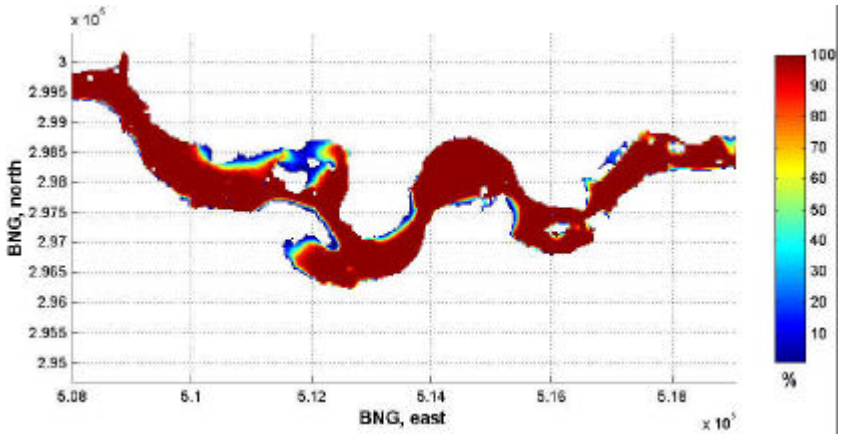

Figure 6. Spatial extent of inundation at flood peak: percentage of simulations in which each cell was inundated. Cells which did not flood in any simulations have been removed for clarity.

The standard deviation and CV of the area of inundation is shown in Figure 7. Maximum standard deviation occurred shortly after the time of maximum inundation extent, as the flood wave moved downstream. The maximum value of 0.17 km^2 was equivalent to ~189 cells. Although the standard deviation in area decreased as the flood wave receded, the CV continued to rise to a maximum of 2.5%. A similar trend was observed in the mean depth of flooding (Figure 8). Although the maximum standard deviation of 0.0225 m was small, the CV continued to rise throughout the simulation to a maximum of 3.2%. Likewise, the CV of volume of flood inundation (Figure 9) continued to rise to a maximum of 4.4%. These figures suggest that variation in predictions become compounded through time. Given flood simulations longer than the 340 hours duration here, variation (and, hence, uncertainty) may further increase.

A different trend was observed in channel outflow discharge (Figure 10). Here, the greatest variation occurred during the rising limb of the hydrograph, before dropping back to a relatively low level. The maximum standard deviation was 3.82 m^3s^{-1}, which represented the maximum CV of 4.5%. High variation in outflow was expected during the rising limb, as this is when flood inundation commences. Variation also occurred during the recession limb of the hydrograph. However, as flood inundation occurred quicker than flood recession, the variation is restricted to a shorted period of time.

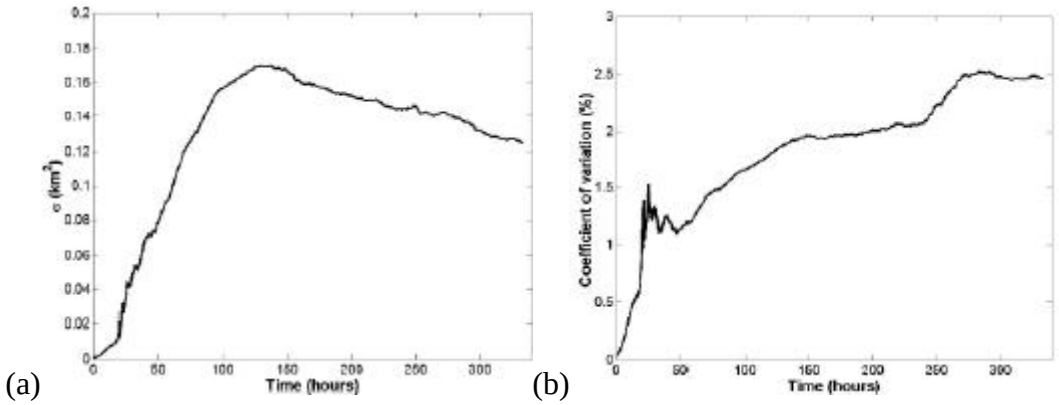

(a) (b)

Figure 7. Variation in flooded area for all simulations: (a) standard deviation; and (b) coefficient of variation.

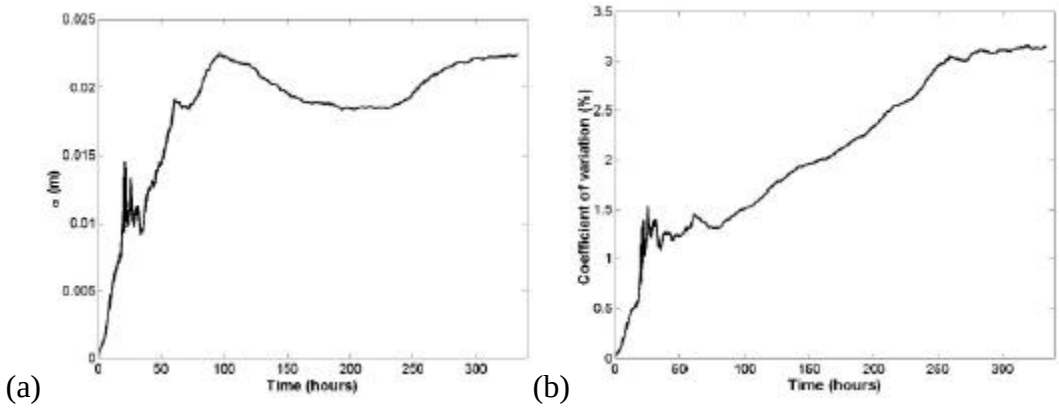

(a) (b)

Figure 8. Variation in mean depth of flooding for all simulations: (a) standard deviation; and (b) coefficient of variation.

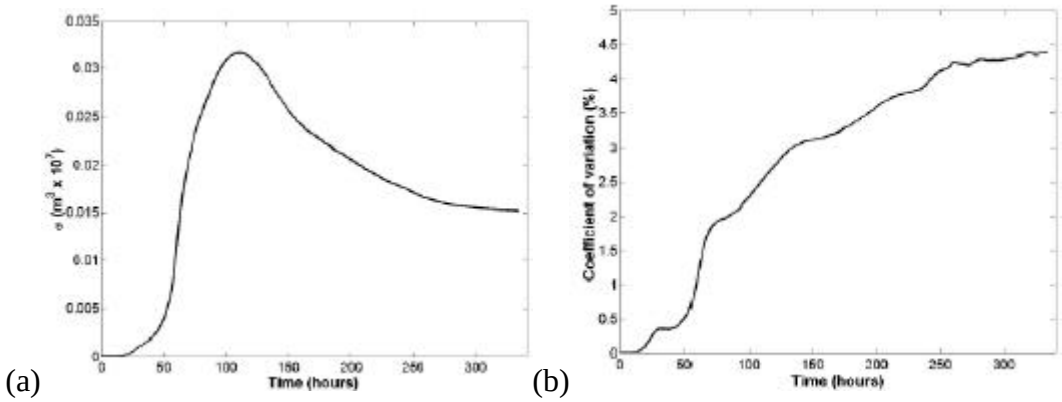

Figure 9. Variation in volume of flooding for all simulations: (a) standard deviation; and (b) coefficient of variation.

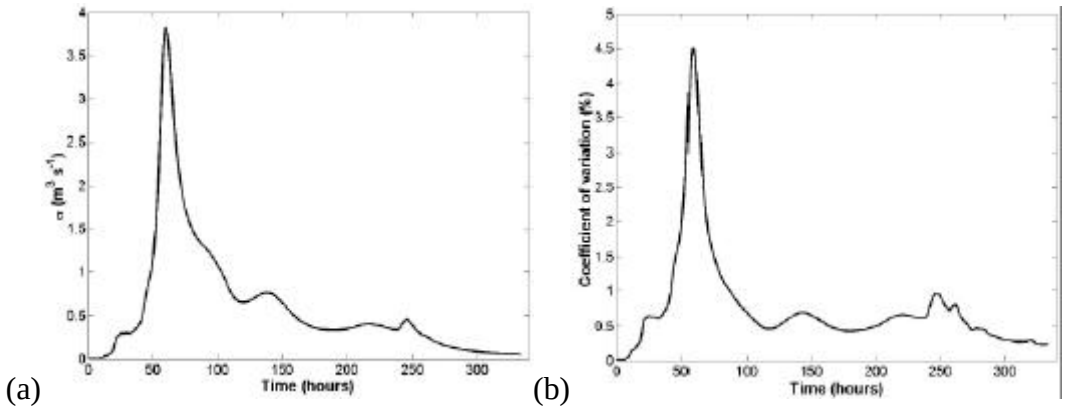

Figure 10. Variation in channel outflow discharge for all simulations: (a) standard deviation; and (b) coefficient of variation.

The mean time of maximum flood depth increased progressively downstream, other than in outlying areas with topographic restrictions. As with the depth at the flood peak, only flooded cells were included in the calculations. High variability in time of maximum flood depth occurred in topographically restricted areas, where the flood wave took longer to reach. The greatest standard deviation in time of maximum depth (Figure 11a) was >100 hours, observed in the area at BNG 512,000 E, 298,500 N. This equated to a CV of ~70% (Figure 11b). Variation in the time of maximum flood depth for the near-channel floodplain is more clearly shown in Figure 12, and for the channel itself in Figure 13. As the flood wave progressed downstream, variation in time of maximum flood depth increased to a maximum standard deviation of ~0.6 hours, which was equivalent to a CV of 0.6%. This uncertainty may have increased further given a longer river reach.

Variations in the time of initial flooding are shown in Figure 14. Areas furthest from the channel that tend to flood last, generally have the largest standard deviation. By using the CV, however, it is clear that there are many areas on the near-channel floodplain in which the time flooding onset has a high degree of variability of 10-20% (Figure 14b). Local (high-frequency) topographic variations were the principal control over where flood water initially flowed. Therefore, the time of initial flooding was particularly influenced by the small changes in local topography across the elevation scenarios. In addition, during the early stages

of the flood event, near-channel topography (especially bank topography) controlled the timing of inundation.

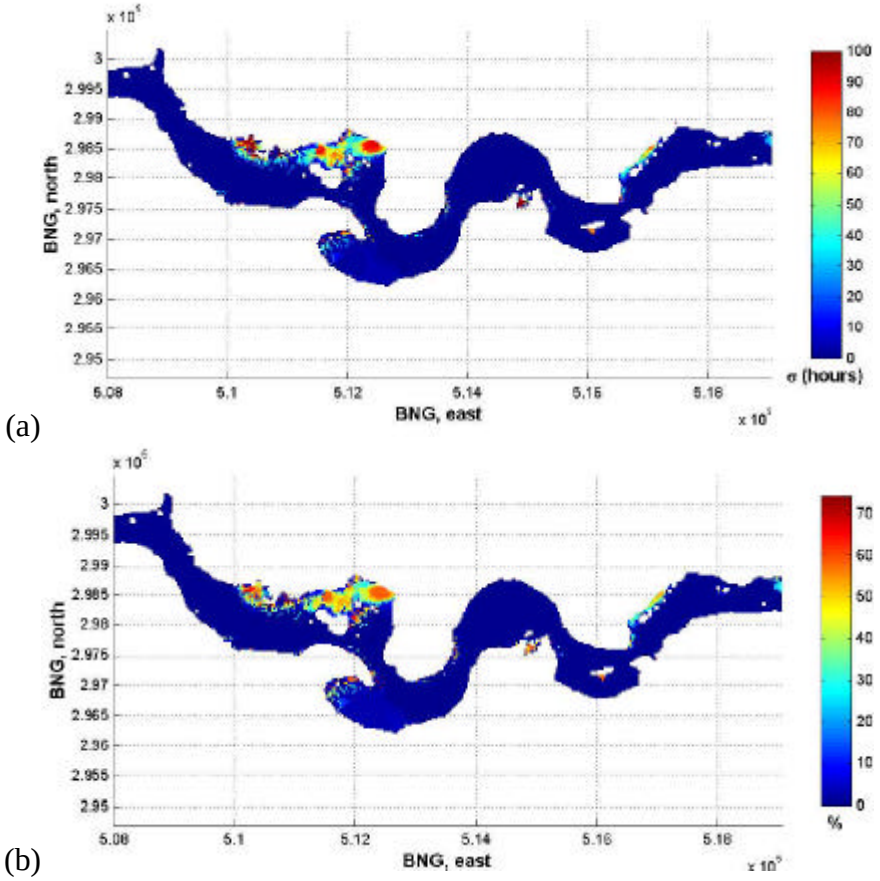

Figure 11. Variation in time of maximum flood for all simulations: (a) standard deviation; and (b) coefficient of variation. Non-flooded cells in each simulation were discounted to avoid skewing the results.

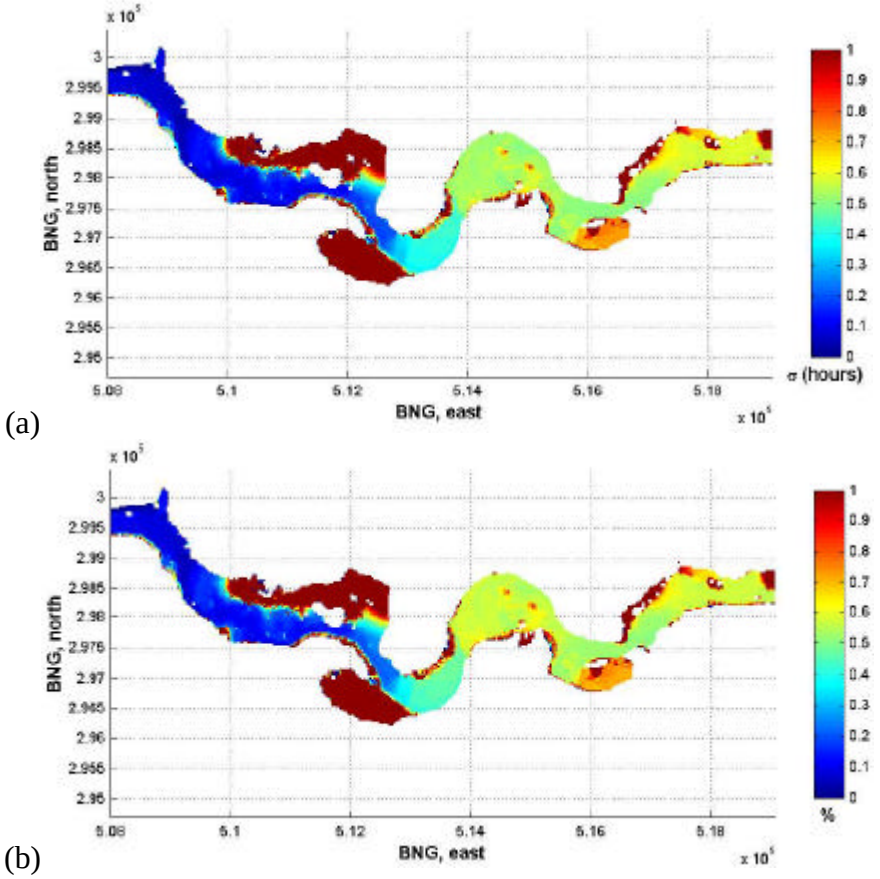

Figure 12. Variation in time of maximum flood for all simulations: (a) standard deviation; and (b) coefficient of variation, scaled between 0 and 1 to highlight the near-channel floodplain.

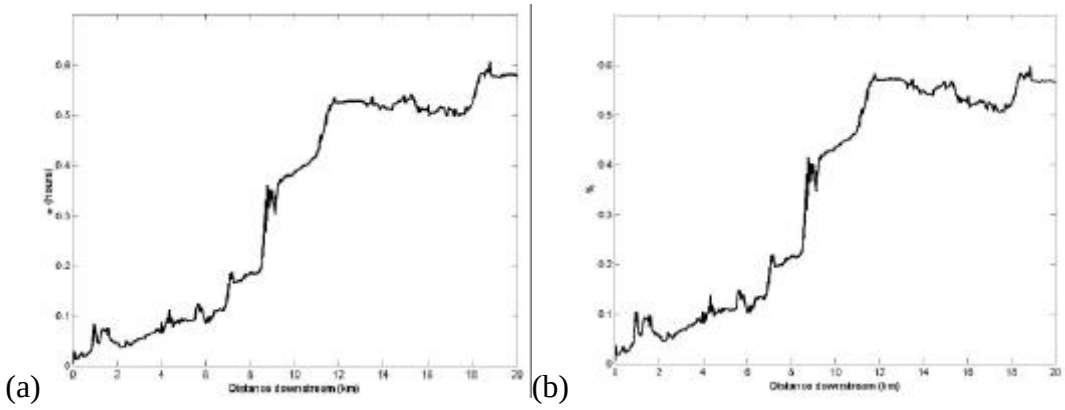

Figure 13. Variation in time of maximum flood for all simulations along the channel: (a) standard deviation; and (b) coefficient of variation.

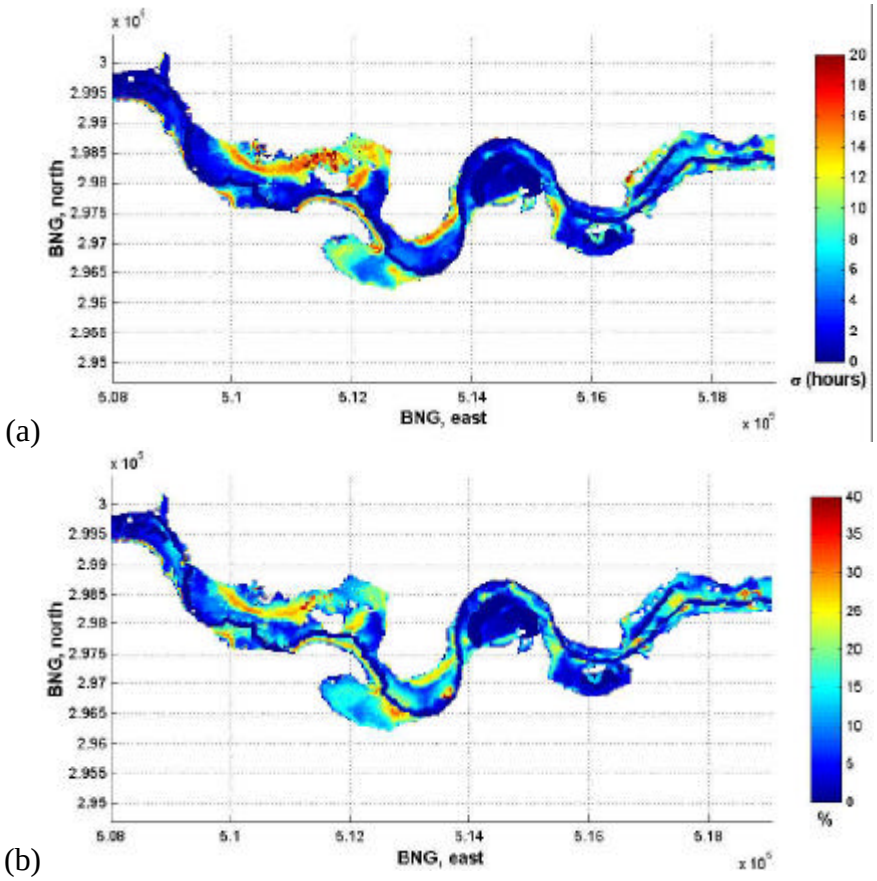

Figure 14. Variation in time of initial flood for all simulations: (a) standard deviation; and (b) coefficient of variation. Non-flooded cells in each simulation were discounted to avoid skewing the results.

6. Discussion

There are large areas where elevation is still uncertain despite additional DGPS data, as indicated by the standard deviation of elevation realisations (Figure 3). Some areas of high standard deviation had access problems, and it was not possible to make DGPS measurements within them. Although a denser network of DGPS may reduce the amount of prediction uncertainty in elevation, this may not be feasible for all areas.

The effects of prediction uncertainty in elevation on the prediction of flood inundation were observed both locally and globally, and increased both through time and with distance downstream. For example, during the simulations the uncertainty in the predicted area of inundation increased to a maximum of 2.5%. For a large flood event, this degree of uncertainty may represent a substantial area. Locally, uncertainty in predicted inundation extent was greatest where elevation gradients were smallest. The location of the flood shoreline is critical for the flood insurance and re-insurance industries, and for the floodplain management. It is in these areas that uncertainty must be reduced.

At the downstream end of the reach, uncertainty in the time of maximum flood depth was 0.6 hours. This was despite the large influence the channel had on the flood wave. For larger reaches, and for flood events where the rising limb lasts longer, this uncertainty may be greater. Away from the channel in areas which were topographically restricted, uncertainty in flood wave timing was greater. This has implications for the real-time modelling of flood

events when the forecasting of the arrival of the flood wave is essential for emergency management.

7. Conclusions

In this paper, the PROFILE^{TM} contour data were obtained from the Ordnance Survey and supplemented by measurements of elevation on the floodplain and along the channel using Differential GPS. The aim was to assess the effect of uncertainty in predictions of elevation on the prediction of inundation extent. The addition of the DGPS measurements to the contour data increased the amount of spatial variation in elevation in the domain, suggesting that the data were more representative of the floodplain.

Sequential Gaussian Simulation was used as a novel method of generating multiple realisations of elevation based on combined contour and DGPS data, whilst maintaining their spatial character. Importantly, each realisation was equally representative of floodplain topography, and model predictions were, therefore, equally valid. The effect of uncertainty in the DEM on the prediction of flood inundation increased both with distance downstream and throughout the simulation. This is important as uncertainty is likely to increase for predictions of flood events at larger scales or of longer duration.

8. Acknowledgements

The authors thank the Ordnance Survey for providing contour data, and Phil Allen of Hampshire County Council for the loan of the Trimble ProXRS unit. Research was funded by a High Performance Computing bursary from the University of Southampton, where simulations were conducted on the Iridis Beowulf cluster.

9. References

BATES, P.D., DE ROO, A.P.J., 2000, A simple raster-based model for flood inundation simulation, *Journal of Hydrology*, **236,** 54-77.

CHOW, V. T., 1959, *Open-Channel Hydraulics* (McGraw-Hill Inc).

CHOW, V. T., Maidment, D.R., Mays, L.W., 1988, *Applied Hydrology* (McGraw-Hill Inc).

DE ROO, A. P. J., VAN DER KNIJFF, J., SCHMUCK, G., BATES, P., 2000, A simple floodplain inundation model to assist in floodplain management, In *New Trends in Water and Environmental Engineering for Safety and Life: Eco-compatible Solutions for Aquatic Environments* (Balkema, Rotterdam).

DEUTSCH, C. V., JOURNEL, A. G., 1998, *GSLIB Geostatistical Software Library and User's Guide, Second Edition*, (Oxford University Press, New York).

GOOVAERTS, P., 1997, *Geostatistics for Natural Resources Evaluation (Applied Geostatistics Series)*, (Oxford University Press, New York).

HORRITT, M. S., BATES, P.D., 2001, Predicting floodplain inundation: raster-based modelling versus the finite element approach, *Hydrological Processes*, **15,** 825-842.